Article

Synthesis, Characterization, and Application of Indolo[3,2-*b*]carbazole Semiconductors

Pierre-Luc T. Boudreault, Salem Wakim, Nicolas Blouin, Michel Simard, Christian Tessier, Ye Tao, and Mario Leclerc

J. Am. Chem. Soc., **2007**, 129 (29), 9125-9136• DOI: 10.1021/ja071923y • Publication Date (Web): 29 June 2007

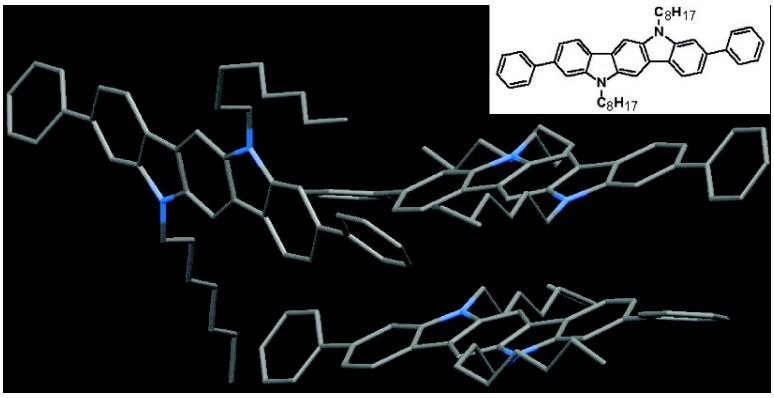

More About This Article

Additional resources and features associated with this article are available within the HTML version:

- Supporting Information
- Links to the 12 articles that cite this article, as of the time of this article download
- Access to high resolution figures
- Links to articles and content related to this article
- Copyright permission to reproduce figures and/or text from this article

View the Full Text HTML

J|A|C|S
ARTICLES
Published on Web 06/29/2007

Synthesis, Characterization, and Application of Indolo[3,2-*b*]carbazole Semiconductors

Pierre-Luc T. Boudreault,[†] Salem Wakim,[†,‡] Nicolas Blouin,[†] Michel Simard,[§] Christian Tessier,[||] Ye Tao,[‡] and Mario Leclerc*[,†]

Contribution from the Canada Research Chair on Electroactive and Photoactive Polymers, Département de Chimie, Université Laval, Quebec City, Quebec, Canada, G1K 7P4, Institute of Microstructural Sciences, National Research Council of Canada, Ottawa, Ontario, Canada, K1A 0R6, Laboratory of X-ray Diffraction, Department of Chemistry, Université de Montréal, Montreal, Quebec, Canada, H3C 3J7, and Département de Chimie, Université Laval, Quebec City, Quebec, Canada, G1K 7P4

Received March 19, 2007; E-mail: mario.leclerc@chm.ulaval.ca

Abstract: The synthesis, characterization, and field-effect transistor (FET) properties of new indolo[3,2-*b*]carbazoles are described. In particular, an extensive characterization of their crystal structures has revealed the importance of the nature of the side chains (alkyl, phenyl, thienyl substituents) on their solid-state organization. These organic materials have exhibited *p*-type FET behavior with hole mobilities as high as 0.2 $cm^2 V^{-1} s^{-1}$ with an on/off current ratio higher than 10^6. Best results were obtained with phenyl-substituted indolo[3,2-*b*]carbazoles since the presence of phenyl substituents seems to allow efficient overlap between the oligomeric molecules. More importantly, FET properties were kept constant during several months in air.

Introduction

Electroactive and photoactive conjugated oligomers and polymers have received much attention over the past two decades because of their great potential in organic electronics.[1] Indeed, they show many advantages over traditional silicon-based materials such as relatively low cost, tunable electronic properties, good mechanical properties, and ease of processing. Some very promising n-type organic semiconductors were recently synthesized,[2] but much of the reported work has been focused on the development of oligomeric and polymeric p-type semiconductors.[3−5] In particular, pentacenes and oligoacenes show very interesting performances as an active semiconductor layer in organic field-effect transistors (OFETs) with hole mobility reaching 2−3 $cm^2 \cdot V^{-1} \cdot s^{-1}$ and on/off current ratios as high as 10^8.[6] The performances can even be higher by using a single crystal in the device;[7] for instance, a charge-carrier mobility of 15 $cm^2 \cdot V^{-1} \cdot s^{-1}$ was achieved using a single crystal of rubrene.[8] These performances are close to those of amorphous silicon, but unfortunately, unsubstituted pentacene and rubrene present a lack of solubility and photostability.

An interesting alternative would be the development of indolo[3,2-*b*]carbazole (IC) derivatives. Indeed, it has already been reported that carbazole[9,10] and indolocarbazole[11−13] derivatives are good hole-transporting units. The first IC-based OFET showed a hole mobility of 10^{-3} $cm^2 V^{-1} s^{-1}$.[11] However, recent studies have shown the great potential of the IC derivatives by reporting a hole mobility up to 0.14 $cm^2 V^{-1} s^{-1}$.[13] The IC unit presents a structure similar to the pentacene, in terms of planarity, with the addition of the two nitrogen atoms on which

[†] Canada Research Chair on Electroactive and Photoactive Polymers, Département de Chimie, Université Laval.
[‡] National Research Council of Canada.
[§] Université de Montréal.
[||] Département de Chimie, Université Laval.

(1) (a) Skotheim, T. A.; Reynolds, J. R. *Handbook of Conducting Polymers*; Taylor & Francis Group: Boca Raton, FL, 2007. (b) Klauk, H. *Organic Electronics*; Wiley-VCH: Weinheim, 2006. (c) Hadziioannou, G.; Malliaras, G. G. *Semiconducting Polymers*; Wiley-VCH: Weinheim, 2007.
(2) a) Tonzola, C. J.; Alam, M. M.; Kaminsky, W.; Jenekhe, S. A. *J. Am. Chem. Soc.* **2003**, *125*, 13548−13558. (b) Letizia, J. A.; Facchetti, A.; Stern, C. L.; Ratner, M. A.; Marks, T. J. *J. Am. Chem. Soc.* **2005**, *127*, 13476−13477. (c) Ando, S.; Murakami, R.; Nishida, J.; Tada, H.; Inoue, Y.; Tokito, S.; Yamashita, Y. *J. Am. Chem. Soc.* **2005**, *127*, 14996−14997.
(3) (a) Murphy, A. R.; Fréchet, J. M. J.; Chang, P.; Lee, J.; Subramanian, V. *J. Am. Chem. Soc.* **2004**, *126*, 1596−1597. (b) McCulloch, I.; Heeney, M.; Bailey, C.; Genevicius, K.; Macdonald, I.; Shkunov, M.; Sparrowe, D.; Tierney, S.; Wagner, R.; Zhang, S. W.; Chabinyc, M. L.; Kline, R. J.; McGehee, M. D.; Toney, M. F. *Nat. Mater.* **2006**, *5*, 328−333. (c) Würthner, F.; Schmidt, R. *ChemPhysChem* **2006**, *7*, 793−797. (d) Payne, M. M.; Parkin, S. R.; Anthony, J. E.; Kuo, C. C.; Jackson, T. N. *J. Am. Chem. Soc.* **2005**, *127*, 4986−4987.
(4) Takimiya, K.; Ebata, H.; Sakamoto, K.; Izawa, T.; Otsubo, T.; Kunugi, Y. *J. Am. Chem. Soc.* **2006**, *128*, 12604−12605.
(5) Miao, Q.; Chi, X.; Xiao, S.; Zeis, R.; Lefenfeld, M.; Siegrist, T.; Steigerwald, M. L.; Nuckolls, C. *J. Am. Chem. Soc.* **2006**, *128*, 1340−1345.
(6) Klauk, H.; Halik, M.; Zschieschang, U.; Schmid, G.; Radlik, W. *J. Appl. Phys.* **2002**, *92*, 5259−5263.
(7) a) Briseno, A. L.; Mannsfeld, S. C. B.; Ling, M. M.; Liu, S.; Tseng, R. J.; Reese, C.; Roberts, M. E.; Yang, Y.; Wudl, F.; Bao, Z. *Nature* **2006**, *444*, 913−917. (b) Briseno, A. L.; Tseng, R. J.; Ling, M. M.; Falcao, E. H. L.; Yang, Y.; Wudl, F.; Bao, Z. *Adv. Mater.* **2006**, *18*, 2320−2324.
(8) Sundar, V.; Zaumseil, J.; Podzorov, V.; Menard, E.; Willett, R.; Someya, T.; Gershenson, M.; Rogers, J. A. *Science* **2004**, *303*, 1644−1646.
(9) (a) Morin, J. F.; Drolet, N.; Tao, Y.; Leclerc, M. *Chem. Mater.* **2004**, *16*, 4619−4626. (b) Li, J.; Dierschke, F.; Wu, J.; Grimsdale, A. C.; Mullen, K. *J. Mater. Chem.* **2006**, *16*, 96−100.
(10) Drolet, N.; Morin, J. F.; Leclerc, N.; Wakim, S.; Tao, Y.; Leclerc, M. *Adv. Funct. Mater.* **2005**, *15*, 1671−1682.
(11) Wakim, S.; Bouchard, J.; Simard, M.; Drolet, N.; Tao, Y.; Leclerc, M. *Chem. Mater.* **2004**, *16*, 4386−4388.
(12) Li, Y.; Wu, Y.; Gardner, S.; Ong, B. S. *Adv. Mater.* **2005**, *17*, 849−853.
(13) Wu, Y.; Li, Y.; Gardner, S.; Ong, B. S. *J. Am. Chem. Soc.* **2005**, *127*, 614−618.

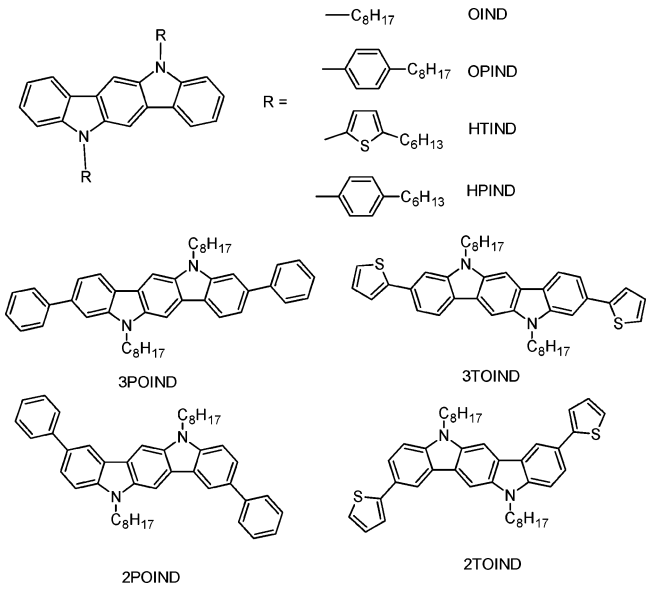

Figure 1. Chemical structure of indolo[3,2-*b*]carbazole-based oligomers.

alkyl or aryl chains can be added to enhance the solubility of the materials. Moreover, functional groups can be added at the 2,8- or 3,9-positions of the indolocarbazole to improve the molecular packing. The presence of reactive groups at either the 2,8- or 3,9-positions can also allow the synthesis of various homopolymers and copolymers with interesting properties.[14]

Along these lines and as shown in Figure 1, we will report the synthesis and the detailed characterization of new indolo-[3,2-*b*]carbazole derivatives. Phenyl and thiophene substituents were introduced at both ends of the IC units or on the nitrogen atoms to improve the hole-transporting properties. The thermal, optical, and electrochemical properties are described as well as a complete X-ray analysis of all single crystals obtained. Measurements in OFETs are also presented with their optimization. In order to better understand the resulting OFET performances, the structures and the morphologies of the vacuum-processed films on the substrates have been carefully characterized. All these studies should shed some light on the relationships between single crystals, vacuum-deposited films, and the OFET performances of indolocarbazole derivatives.

Results and Discussion

Synthesis of Indolo[3,2-*b*]carbazoles. The syntheses of 5,11-dioctylindolo[3,2-*b*]carbazole (OIND), 5,11-bis(*p*-octylphenyl)indolo[3,2-*b*]carbazole (OPIND), 5,11-bis(*p*-hexylphenyl)indolo[3,2-*b*]carbazole (HPIND), and 5,11-bis(5-hexylthiophene)indolo[3,2-*b*]carbazole (HTIND) have already been reported in the literature.[13,15] The synthetic pathways for 3,9- or 2,8-diphenyl-5,11-dioctylindolo[3,2-*b*]carbazole (3POIND and 2POIND) and 3,9- or 2,8-di(thien-2′yl)-5,11-dioctylindolo-[3,2-*b*]carbazole (3TOIND and 2TOIND) are described in Figure 2. First, 3,9- or 2,8-dibromo-5,11-dihydroindolo[3,2-*b*]carbazole has been synthesized following procedures well described in the literature,[12] leading to compounds **1** and **2**. Then, these compounds were alkylated via a phase-transfer condensation with *n*-octyl bromide and aqueous NaOH in DMSO in the presence of benzyltriethylammonium chloride to afford compounds **3** and **4**. Long alkyl chains were chosen to provide good solubility and to enhance the molecular self-organization of the oligomers.

The synthesis of 3TOIND and 2TOIND was achieved using a Stille cross-coupling reaction[16] because it is known that the Stille reaction is more effective than the Suzuki reaction for thiophene units. Thus, compounds **3** and **4** were used as starting materials for a standard Stille cross-coupling reaction with 2-(tributylstannyl)thiophene to provide compounds **5** (3TOIND) and **6** (2TOIND). It has been shown over the years that the introduction of a thiophene unit at both ends creates a material that is nearly flat and might provide a tight packing of the oligomer.[17]

The indolocarbazole oligomers containing a phenyl unit at both ends were prepared by Suzuki cross-coupling following procedures reported by Buchwald et al.[18] The oligomers **7** (3POIND) and **8** (2POIND) were obtained from compounds **3** and **4** and phenylboronic acid. Recently, the introduction of phenyl substituents has been used in organic semiconductors with very interesting performances.[4]

Thermal Properties. The thermal properties of the oligomers were determined by thermogravimetric analysis (TGA) and differential scanning calorimetry (DSC). As shown in Table 1, TGA analyses show that all the compounds are thermally stable up to, at least, 280 °C under a nitrogen atmosphere. The decomposition process was completed for all oligomers when the temperature was raised above 500 °C.

The thermal transitions of the oligomers have been studied by DSC and are also reported in Table 1. All oligomers show an important melting endotherm and the corresponding crystallization endotherm except for the HTIND which was not observed during the time of the experiment. It should be noted that a second endotherm and crystallization exotherm were observed for the 3TOIND and for OIND, those minor transitions being probably due to some disorder created by the long alkyl chains. This first transition observed during the heating occurred at 103 °C for 3TOIND and at 84 °C for OIND.

Optical and Electrochemical Properties. The UV−visible absorption properties of all synthesized oligomers have been also investigated and are reported in Table 2. The spectra have been taken in CH_2Cl_2 solution and on vacuum-deposited thin films.

The UV−visible absorption maximum of an oligomer is closely associated with its conjugation length, meaning that a longer conjugation length for a particular oligomer will lead to a red shift of the maximum of absorption. For instance, the compounds containing either thiophene or phenyl groups at both ends have a longer conjugation length than the OIND that do not contain any aryl end group; therefore, their absorption maxima are red-shifted. As expected, the indolocarbazole derivatives with thiophene units at the ends have a longer conjugation length than their corresponding phenyl-capped

(14) (a) Blouin, N.; Leclerc, M.; Vercelli, B.; Zecchin, S.; Zotti, G. *Macromol. Chem. Phys.* **2006**, *207*, 175−182. (b) Blouin, N.; Michaud, A.; Wakim, S.; Boudreault, P. L. T.; Leclerc, M.; Vercelli, B.; Zecchin, S.; Zotti, G. *Macromol. Chem. Phys.* **2006**, *207*, 166−174. (c) Li, Y.; Wu, Y.; Ong, B. S. *Macromolecules* **2006**, *39*, 6521−6527.
(15) Belletête, M.; Blouin, N.; Boudreault, P. L. T.; Leclerc, M.; Durocher, G. *J. Phys. Chem. A* **2006**, *110*, 13696−13704.
(16) Stille, J. K. *Angew. Chem., Ed. Engl.* **1986**, *25*, 508−524.
(17) (a) Meng, H.; Sun, F.; Goldfinger, M. B.; Jaycox, G. D.; Li, Z.; Marshall, W. J.; Blackman, G. S. *J. Am. Chem. Soc.* **2005**, *127*, 2406−2407. (b) Halik, M.; Klauk, H.; Zschieschang, U.; Schmid, G.; Ponomarenko, S.; Kirchmeyer, S.; Weber, W. *Adv. Mater.* **2003**, *15*, 917−922.
(18) Walker, S. D.; Barder, T. E.; Martinelli, J. R.; Buchwald, S. L. *Angew. Chem., Int. Ed.* **2004**, *43*, 1871−1876.

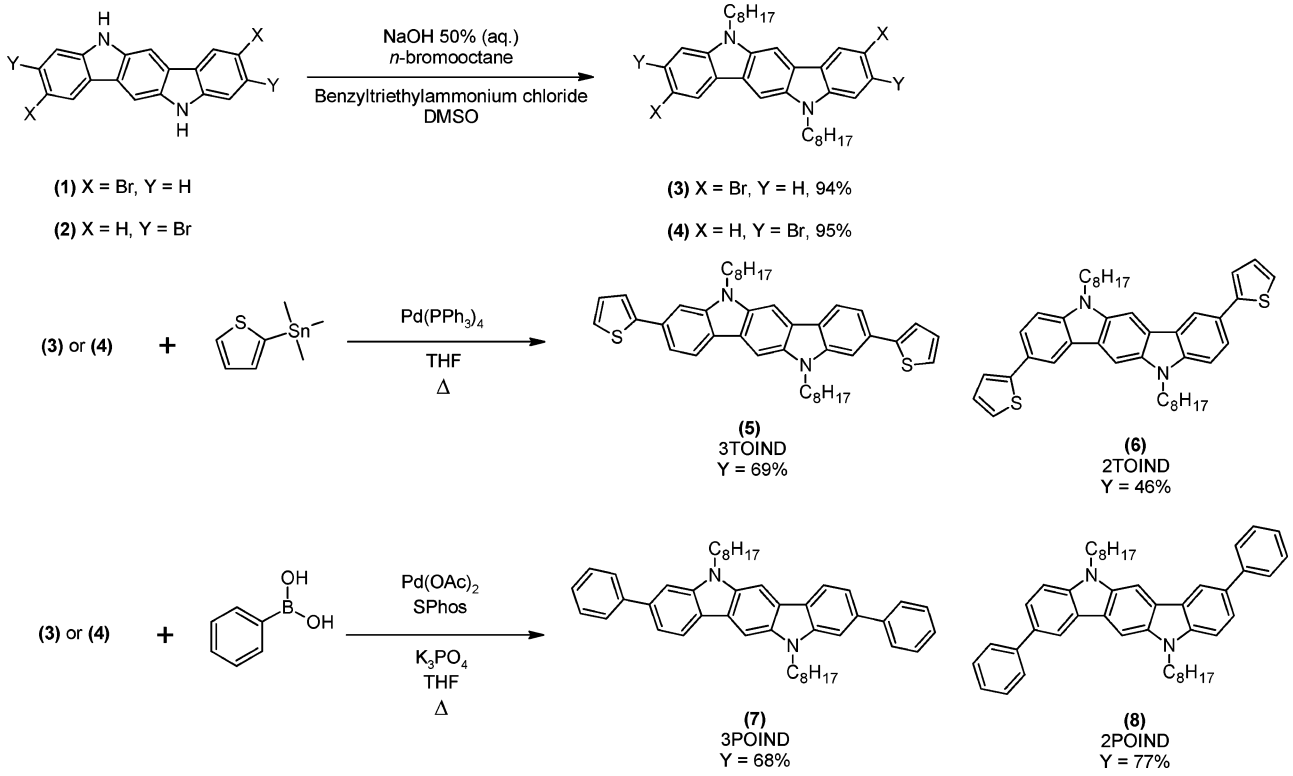

Figure 2. Synthesis of the oligomers. SPhos: 2-dicyclohexylphosphino-2′,6′-dimethoxydiphenyl.

Table 1. Thermal Properties of Oligomers

oligomer	T_{deg}[a] [°C]	T_m[b] [°C]	T_c[b] [°C]
OIND	280	101 (84)	
OPIND	374	131	
HPIND	380	161	123
HTIND	390	109	–
3POIND	410	237	196
2POIND	346	193	150
3TOIND	395	228 (103)	200 (80)
2TOIND	400	203	139

[a] Degradation temperature (T_{deg}) observed from TGA corresponding to 5% weight loss at 10 °C·min^{-1} under nitrogen flow. [b]Melting temperature (T_m) and crystallization temperature (T_c) observed from DSC at 10 °C·min^{-1} under nitrogen flow.

molecules. Substitution at positions 3 and 9 of the indolocarbazole derivatives also leads to a longer conjugation length compared to the substitution at positions 2 and 8. Therefore, the UV−visible absorption maximum for 3POIND is 366 nm compared to an absorption maximum of 349 nm for 2POIND. One can also see in Table 2 that the replacement of the alkyl chains on the nitrogen atoms by thiophene (HTINC) or phenyl units (HPINC, OPINC) induces a small blue shift of the absorption bands.

On the other hand, the absorption spectra of all vacuum-deposited oligomer thin films show a red shift of the longest wavelength absorption maxima relative to those obtained in solution (Figure 3). This red shift can be attributed to a better delocalization due to π-stacking, indicating strong intermolecular interaction in the thin films.[5,19] However, in the particular case of 3POIND and 3TOIND, the main absorption bands of vacuum-deposited thin films are blue-shifted by about 10 nm in comparison with those measured in a dilute solution (Figure 3a). The formation of H-aggregates is supposed here which implies excitonic coupling between adjacent molecules in a closely packed structure.[10,20] The optical bandgaps estimated from the absorption edges of the vacuum-deposited thin films spectra range from 2.6 to 2.8 eV, which is about 1 eV wider than that of pentacene.[21] Cyclic voltammetry experiments showed one quasi-reversible oxidation wave within the range of the solvent/electrolyte window for all oligomers. The results are summarized in Table 2. The highest occupied molecular orbital (HOMO) energy levels, estimated from the oxidation onset,[22] vary from 5.4 to 5.6 eV from vacuum. These HOMO levels are lower than those of pentacene[23] and of many thiophene derivatives,[19] indicating a better oxidation stability[24] for these indolocarbazole-based oligomers. Moreover, the HOMO energy levels of these oligomers match also quite well with the work function of a gold electrode (5.1 eV).[25]

Crystallographic Analyses. The single crystals were grown by recrystallization in common organic solvents. For instance, 3POIND, 2POIND, and HTIND were recrystallized using dichloromethane and hexanes. We used only hexanes to afford the single crystals for OIND, OPIND, and HPIND. Unfortunately, we were unable to obtain single crystals with 3TOIND and 2TOIND despite numerous attempts. All crystallographic data (Crystallographic information files) for these oligomers can

(19) Heeney, M.; Bailey, C.; Genevicius, K.; Shkunov, M.; Sparrowe, D.; Tierney, S.; McCulloch, I. *J. Am. Chem. Soc.* **2005**, *127*, 1078−1079.
(20) Sun, Y.; Ma, Y.; Liu, Y.; Lin, Y.; Wang, Z.; Wang, Y.; Di, C.; Xiao, K.; Chen, X.; Qiu, W.; Zhang, B.; Yu, G.; Hu, W.; Zhu, D. *Adv. Funct. Mater.* **2006**, *16*, 426−432.
(21) (a) Yasuda, T.; Goto, T.; Fujita, K.; Tsutsui, T. *Appl. Phys. Lett.* **2004**, *85*, 2098−2100. (b) Xiao, K.; Liu, Y.; Qi, T.; Zhang, W.; Wang, F.; Gao, J.; Qiu, W.; Ma, Y.; Cui, G.; Chen, S.; Zhan, X.; Yu, G.; Qin, J.; Hu, W.; Zhu, D. *J. Am. Chem. Soc.* **2005**, *127*, 13281−13286.
(22) Thompson, B. C.; Kim, Y. G.; Reynolds, J. R. *Macromolecules* **2005**, *38*, 5359−5362.
(23) Meng, H.; Bendikov, M.; Mitchell, G.; Helgeson, R.; Wudl, F.; Bao, Z.; Siegrist, T.; Kloc, C.; Chen, C. H. *Adv. Mater.* **2003**, *15*, 1090−1093.
(24) Meng, H.; Zheng, J.; Lovinger, A. J.; Wang, B. C.; Patten, P. G. V.; Bao, Z. *Chem. Mater.* **2003**, *15*, 1778−1787.
(25) Katz, H. E.; Bao, Z. *J. Phys. Chem. B* **2000**, *104*, 671−678.

Table 2. Optical Absorption Maxima (λ_{max}) and Electrochemical Properties of Oligomers

oligomer	λ_{max} [nm] solution[a]	λ_{max} [nm] thin film[b]	E_g [eV] thin film[b]	$E_{peak\ ox}$ [V, vs SCE][c]	E_{HOMO} [eV][d]
OIND	325, 342, 395, 418	327, 400, 428	2.65	0.81 (0.71)	5.41
OPIND	322, 338, 388, 409	323, 341,415	2.80	0.93 (0.82)	5.52
HPIND	322, 339, 388, 409	326, 342, 391, 416	2.87	0.93 (0.82)	5.52
HTIND	320, 336, 380, 398	326, 345, 402	2.71	1.01 (0.92)	5.62
3POIND	366, 408, 433	356, 420, 450	2.65	0.82 (0.73)	5.43
2POIND	320, 349, 404, 428	326, 416, 439	2.73	0.79 (0.69)	5.39
3TOIND	383, 442	374, 400, 416, 464	2.59	0.85 (0.75)	5.45
2TOIND	334, 353, 411, 435	340, 360, 422,447	2.70	0.79 (0.69)	5.39

[a] Measurements performed in CH_2Cl_2. [b]Measurements performed on 300 Å thin films vacuum-deposited on quartz. [c]SCE: standard calomel electrode. The values in parentheses correspond to the oxidation peak onset. [d]Ionization potential (E_{HOMO}; HOMO: highest occupied molecular orbital) measured from the cathodic onset.

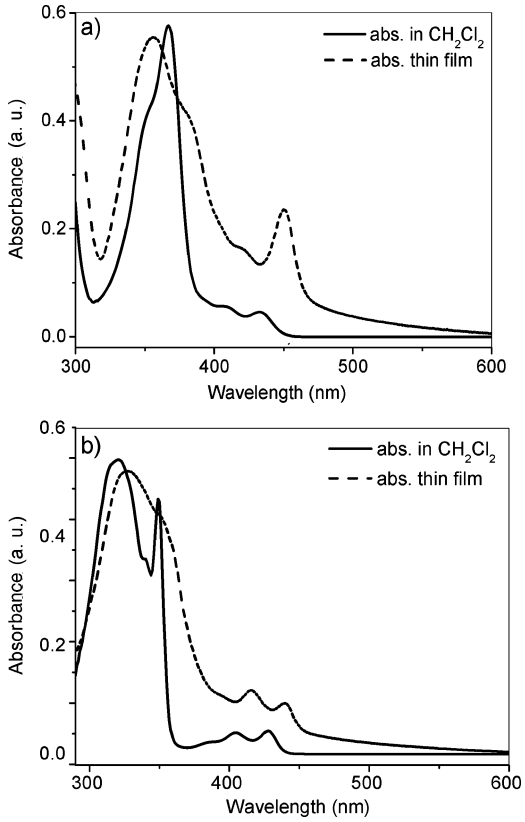

Figure 3. UV−vis absorption spectra of (a) 3POIND and (b) 2POIND in solution and vacuum-deposited thin films.

be found in the Supporting Information. First, X-ray crystallographic analysis of OIND shows that the molecules possess strong cofacial $\pi-\pi$ stacking (face-to-face interaction) along the *b*-axis with a minimal intermolecular distance of 3.49 Å. The molecules also adopt a herringbone structure along the *c*-axis in such a way that each indolocarbazole has edge-to-face contacts of 3.75 Å with two molecules from the adjacent stacks (Figure 4). We note here that the packing mode of OIND is somehow similar to that reported for 5,11-dioctyl-6,12-dimethylindolo[3,2-*b*]carbazole,[11] except the fact that the adjacent molecules along the *b*-axis are coplanar for the last indolocarbazole. The minimal intermolecular distance between coplanar adjacent indolocarbazoles is about 3.74 Å (Figure 4).

Figure 5 shows the crystal structure of OPIND. The shortest intermolecular distances are 3.44 Å in the π-staked arrays (along the *c*-axis) and 3.55 Å between adjacent coplanar indolocarbazole cores (along the *a*-axis). The phenyl pendant groups of each indolocarbazole are tilted in the same direction, at torsion angles of 50°−78° with respect to the indolocarbazole backbone. It is important to note that additional interactions between neighboring indolocarbazole are provided by the phenyl side chains. Between two adjacent π-staked indolocarbazoles, there are several phenyl−indolocarbazole and phenyl−phenyl close contacts (3.6−4.1 Å C-to-C) (Figure 5B). Each indolocarbazole also interacts with two indolocarbazole molecules from the adjacent stack through phenyl−indolocarbazole short contacts (3.5−3.8 Å C-to-C) (Figure 5C). This efficient packing could allow the charges to circulate in a sort of two-dimensional arrangement. Thus, the OPIND packing is similar but much more compact than the one obtained with 5,11-dioctyl-6,12-dimethylindolo[3,2-*b*]carbazole which could partially explain its higher hole mobility (0.12 versus 0.001 $cm^2\ V^{-1}\ s^{-1}$) in OFETs.[11,13]

We note here that the molecular packing of these indolo-[3,2-*b*]carbazole derivatives with *n*-octyl side chains consists of alternating layers of π-stacked aromatic backbones and alkyl side chains. This kind of organization is related, to a large extent, to the favorable attractive interactions between the alkyl side chains and allows, as detailed above, a bidirectional electronic coupling in the solid.[26] The use of shorter alkyl chains reduces the self-assembly properties of these alkyl side chains and allows the aromatic backbone to direct the supramolecular assembly.

In fact, the crystallographic data of the HPIND (Figure 6) show a completely different packing from the one obtained with OPIND. First, the alkyl side chains are isolated one from the other; the aromatic planes of the cofacial indolocarbazole are approximately 10 Å apart (along the *a*-axis), which prevents any face-to-face interactions (Figure 6A). All the lateral phenyl groups are parallel and reclined to around 66° with respect to the indolocarbazole core. The second significant difference concerns the HPIND layers parallel to the *ab*-plane. They are shifted one compared to the other, and the molecules of two adjacent layers adopt a herringbone geometry along the *c*-axis as shown in Figure 6B. This kind of organization makes these layers highly interdigitated and creates strong electronic interactions between them. Thus, as shown in Figure 6C, each phenyl (from layer 1) has several short phenyl−indolocarbazole contacts (3.5−3.9 Å) with three molecules from the adjacent layer (layer 2), and phenyl−phenyl contacts (3.5−4.1 Å) with two molecules from the further layer (layer 3). This creates a sort of three-dimensional network of short C_{Ar}-to-C_{IC} and C_{Ar}-to-C_{Ar} distances in the solid which could produce high charge carrier mobility in OFETs. We note here that the shortest C_{IC}-to-C_{IC} distance is higher than 4.1 Å; therefore one can suppose that

(26) Anthony, J. E. *Chem. Rev.* **2006**, *106*, 5028−5048.

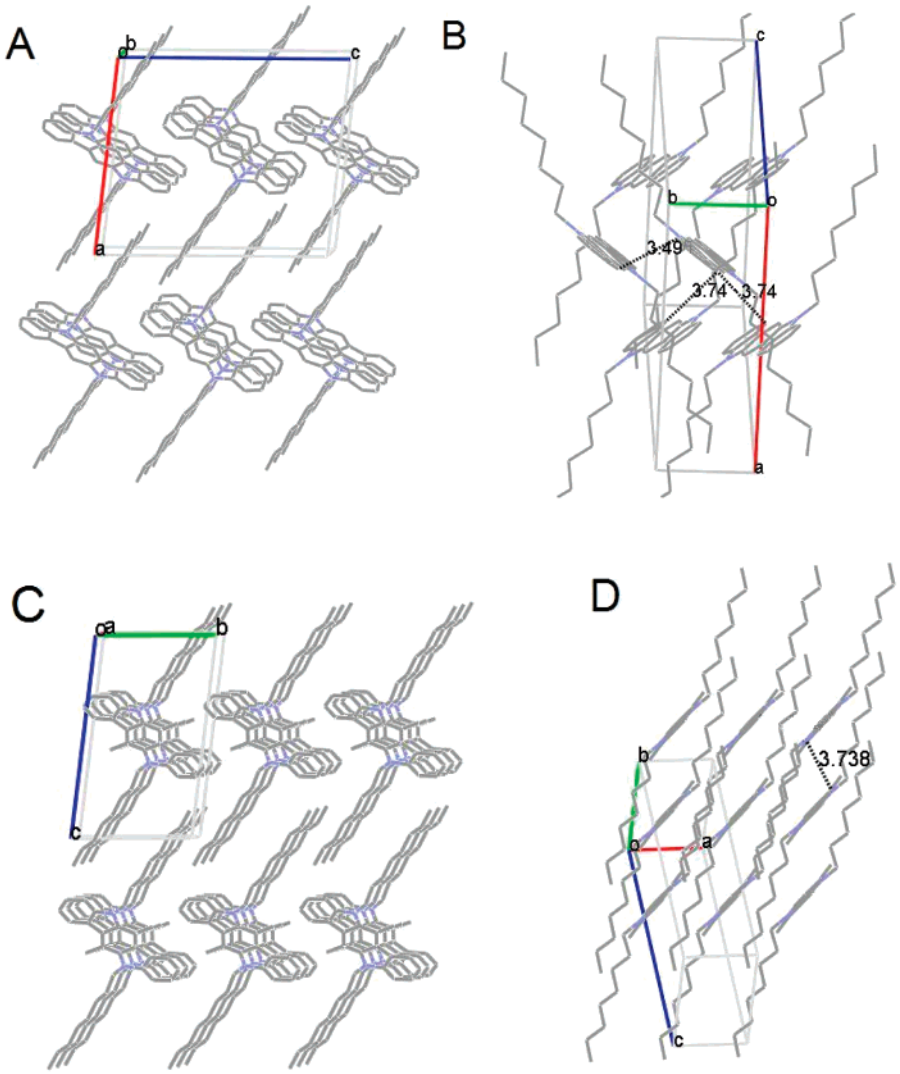

Figure 4. Crystal structures of 5,11-dioctylindolo[3,2-*b*]carbazole (OIND) (A, B) and 5,11-dioctyl-6,12-dimethylindolo[3,2-*b*]carbazole (C, D).[11] Hydrogen atoms have been removed to clarify the view.

the phenyl side chains play an essential role in the electronic coupling in this case.

It is interesting to evaluate the effect of the substitution of the phenyl units by thiophene units by comparing the HTIND crystallographic data with those obtained with HPIND. As shown in Figure 7, the HTIND has many similarities in packing to the HPIND. The thiophene planes are twisted to 65° and 72° with respect to the indolocarbazole core. We observed a similar layered structure with long cofacial indolocarbazole distances of 9.6 Å along the *b*-axis and isolated alkyl side chains. The highly interdigitated layers again allow each thiophene to have several short contacts with three indolocarbazole molecules from the adjacent layer (3.6−3.9 Å) (Figure 7A). The primary difference in the packing of HTIND comes from the adjacent molecules within each layer that adopt a herringbone geometry with C-to-C distances of 3.95 Å. The interlayer C_{IC}-to-C_{IC} distances (about 3.48 Å) are also shorter than those measured for the HPIND (4.16 Å). In this case, both indolocarbazole cores and thiophene side chains provide a three-dimensional electronic coupling in the solid.

A single crystal for 3POIND was also obtained, and the structural arrangement (Figure 8) is very similar to that observed in OIND. Both types of face-to-face and edge-to-face interactions between the indolocarbazole cores are observed in the solid-state assembly. The minimal cofacial intermolecular distance is 3.62 Å, slightly higher than the one measured for OIND (3.49 Å) probably due to the presence of a twisted lateral phenyl (34−36°). Each indolocarbazole has short edge-to-face contacts (3.5−3.6 Å) with two indolocarbazole molecules from the adjacent stack. These edge-to-face interactions are shorter than those calculated for OIND and implicate four rings from each molecule, compared to only two rings in the case of OIND. This kind of organization creates an extremely strong bidirectional electronic coupling in the solid, parallel to the *ac* single-crystal plane.

The position of the lateral phenyl ring on the indolo[3,2-*b*]-carbazoles has limited impact on the general packing mode; the 2POIND and 3POIND molecules adopt a relatively similar organization in the crystal (Figure 9). However, important differences which could have a significant effect on the electronic properties are noted here. The lateral phenyl groups are slightly twisted (5°−6°) which could explain the short cofacial intermolecular distances of 3.48 Å. The edge-to-face interactions occur, as in 3POIND, between one indolocarbazole and two neighbors from each adjacent stack (3.6−3.9 Å). In this case, only two rings from each molecule are implicated.

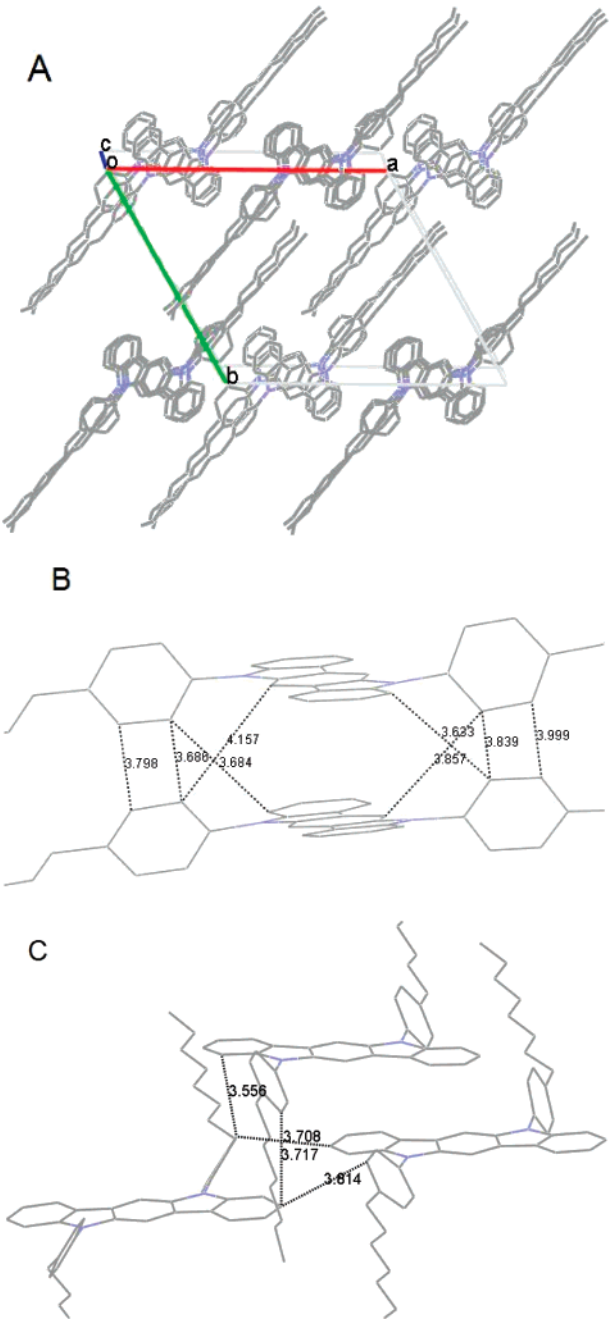

Figure 5. Crystal structures of 5,11-bis(*p*-octylphenyl)indolo[3,2-*b*]carbazole (OPIND). Hydrogen atoms have been removed to clarify the view.

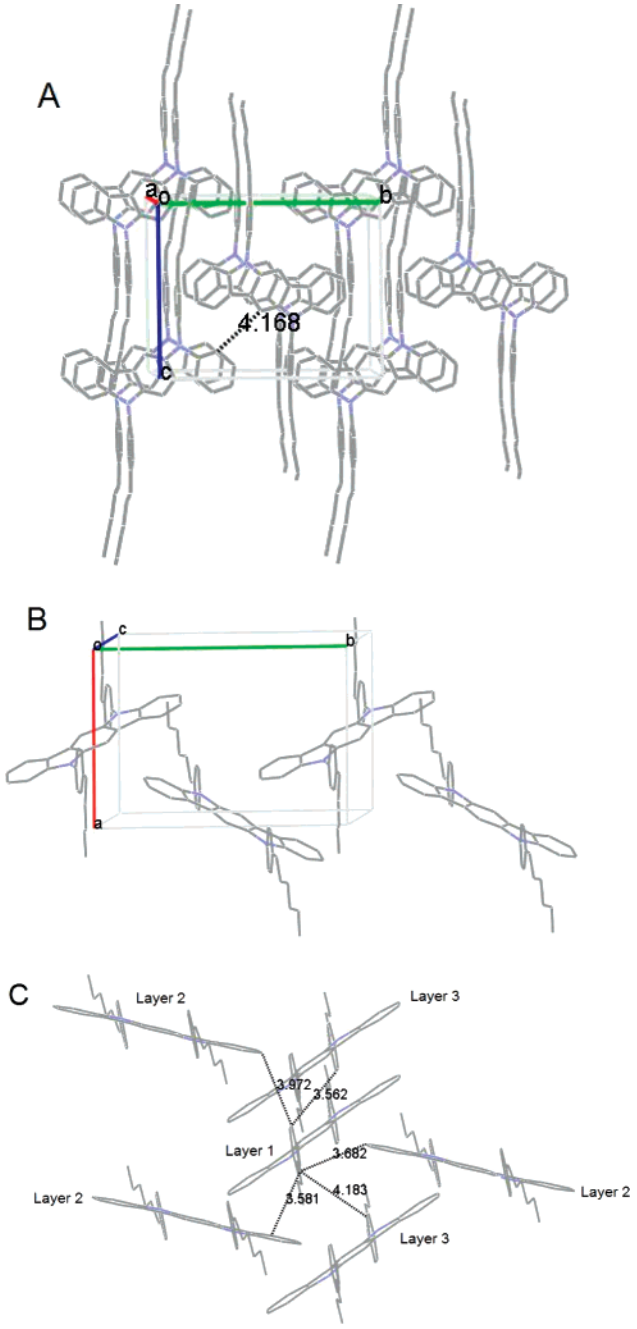

Figure 6. Crystal structures of 5,11-bis(*p*-hexylphenyl)indolo[3,2-*b*]carbazole (HPIND). Hydrogen atoms have been removed to clarify the view.

The 2POIND π-stacked molecules show a displacement along the long and short axes, whereas the displacement is only along the short axis for 3POIND.

This study on the single-crystal structures of these indolocarbazole derivatives allows us to draw several generalities concerning the indolocarbazole derivative packing. The length of the alkyl side chains has a great impact on the crystal packing probably due to their self-assembly properties. The *n*-octyl chains induce the formation of π-stacked layers separated by interdigitated alkyl chain layers. The use of shorter alkyl chains allows the indolocarbazole cores to dictate the nature of the intermolecular interactions, typically characterized as edge-to-face interactions. The minimal face-to-face and edge-to-face intermolecular distances are about 3.5 Å which is favorable to produce high charge carrier mobility by intermolecular hopping.[27] We have also noted that the functionalization of the nitrogen atoms with different aryl groups having the same size or the substitution of the indolocarbazole backbones at the 2,8- or 3,9-positions with relatively similar groups has a limited impact on the solid packing.

Structural and Morphological Characteristics of Indolo[3,2-*b*]carbazoles. The film structure of these indolo[3,2-*b*]-carbazole derivatives was studied by X-ray diffraction (XRD) in reflection mode for 30 nm vacuum-deposited films. Different pretreated SiO_2/Si substrate and different substrate deposition temperatures were investigated in order to evaluate the effect of these two parameters on the ability of these oligomers to form ordered structures in thin films. Moreover, the comparison

(27) Horowitz, G. *J. Mater. Chem.* **1999**, *9*, 2021−2026.

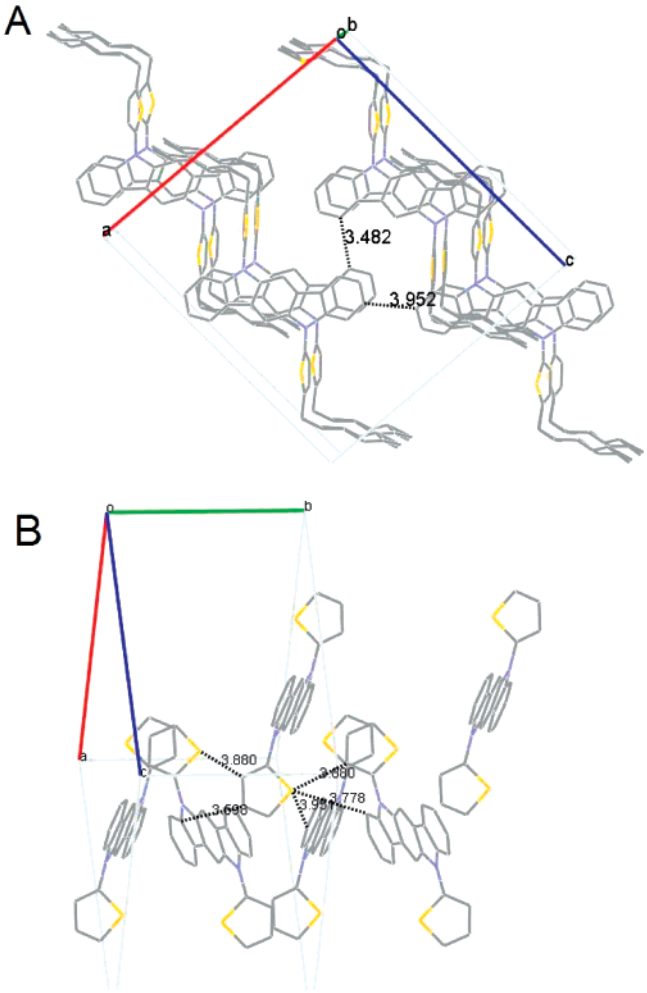

Figure 7. Crystal structures of 5,11-bis(5-hexylthien-2′-yl)indolo[3,2-*b*]-carbazole (HTIND). Hydrogen atoms have been removed to clarify the view.

of XRD data with the single-crystal structures will provide important information about the molecular orientation in thin films. The XRD spectrum of 3POIND, deposited at a substrate temperature (deposition temperature or T_d) fixed at 25 °C, shows a primary diffraction peak at $2\theta = 5.26°$, with the second- and third-order diffraction peaks indicating that this oligomer forms highly ordered molecular structures in thin films even at low T_d (Figure 10). Using the powder pattern simulation from the single-crystal structure, the first reflection peak in the 3POIND film is indexed as (0 1 0), and the remaining, higher order, as (0 *k* 0). The presence of (0 *k* 0) planes and the absence of any other reflection mean that the crystals in the thin film are oriented with the (0 *k* 0) plane, i.e., the *ac* plane parallel to the substrate surface (Figure 8A). The interplanar *d*-spacing (16.8 Å) calculated from the primary diffraction peak is slightly shorter than the *b*-axis length observed in the crystal structure (17.6 Å), probably due to the α-angle (108°) of the single-crystal unit. Therefore, this confirms that molecules in 3POIND adopt an edge-on orientation relative to the substrate with the alkyl chains pointed toward the surface. This kind of molecular packing, where the directions of the face-to-face and edge-to-face interactions are parallel to the substrate surface, is known to produce high charge carrier mobility in OFETs.[28] We note

(28) Sirringhaus, H.; Brown, P. J.; Friend, R. H.; Nielsen, M. M.; Bechgaard, K.; Langeveld-Voss, B. M. W.; Spiering, A. J. H.; Janssen, R. A. J.; Meijer, E. W.; Herwig, P.; Leeuw, D. M. *Nature* **1999**, *401*, 685−688.

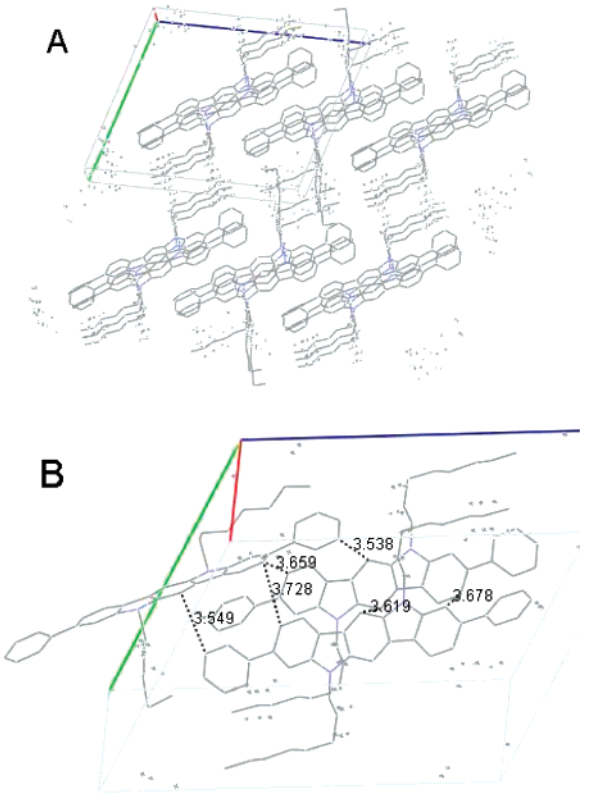

Figure 8. Crystal structure of 3,9-diphenyl-5,11-dioctylindolo[3,2-*b*]-carbazole (3POIND). Hydrogen atoms have been removed to clarify the view.

here a second set of diffraction peaks up to third-order ($2\theta =$ 5.50°, 11°, and 16.5°) when 3POIND was deposited at a substrate temperature between 75 and 100 °C (Figure 10). The peak intensities of the second set increase at higher substrate temperatures; at $T_d = 150$ °C, the first set of diffraction peaks becomes negligible and only the second one represents the thin film structure. However, the calculated *d*-spacing from the second diffraction set is 16 Å, about 1 Å shorter than the one measured for the first diffraction set. This small difference indicates a minor change in the molecular orientation rather than a total change in the packing structure of the 3POIND thin films. It will be shown that this difference could have an effect on the film electrical performances.

The 2POIND film deposited at $T_d = 25$ °C exhibits one dominant set of Bragg reflections up to the third-order reflections ($2\theta = 6.10°$, 12.13°, and 18.26°) indicating a high degree of ordering (Figure 11). These reflections correspond well with the (0 *k l*) reflections from the single-crystal data. The calculated *d*-spacing of 14.5 Å is quite similar to the interlayer distance as obtained from the single crystal and therefore confirms that the indolocarbazole backbone layers are parallel to the surface with an edge-on orientation of the molecules (Figure 9). Once again, the face-to-face and edge-to-face interactions have an appropriate orientation to produce high charge carrier mobility in OFETs. There is also a second set of diffraction peaks (2θ = 6.52°, 13.12°, and 19.7°) in this case that emerged when 2POIND was deposited at T_d between 50 and 75 °C, but contrary to 3POIND, they disappeared at $T_d = 100$ °C. This second set, which could be the signature of more tilted molecules on the surface, does not have a notable effect on the device performances. The X-ray diffraction pattern of 3TOIND thin films

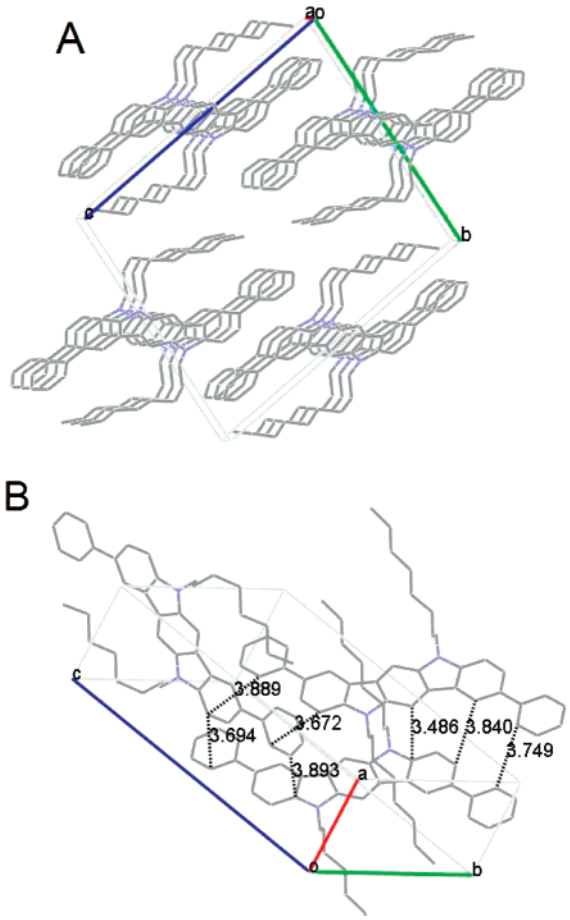

Figure 9. Crystal structure of 2,8-diphenyl-5,11-dioctylindolo[3,2-*b*]-carbazole (2POIND). Hydrogen atoms have been removed to clarify the view.

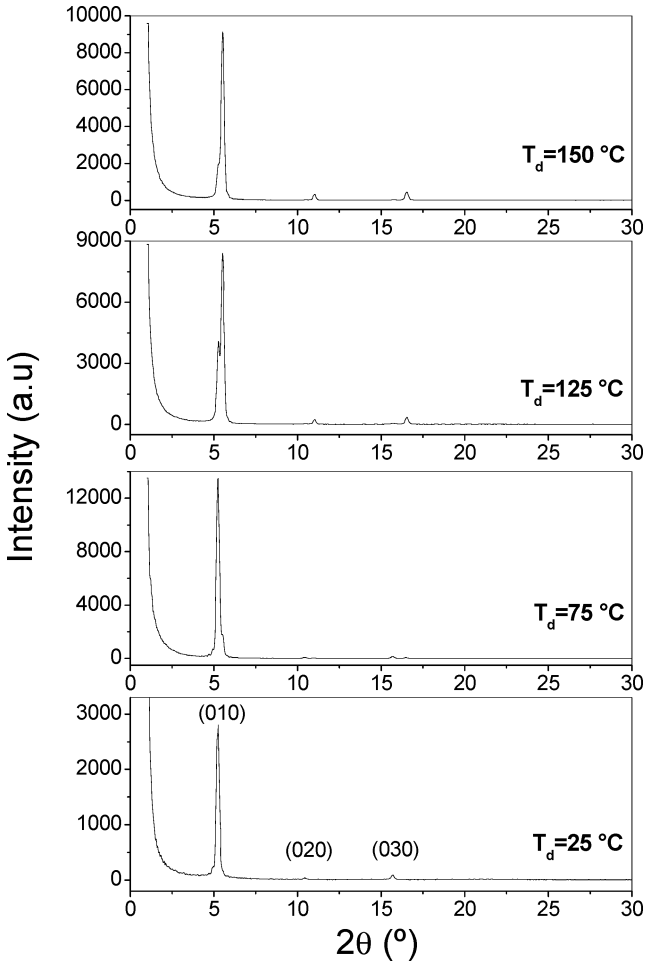

Figure 10. XRD patterns of 3POIND thin films vacuum-deposited on OTS-treated SiO_2/Si at different substrate temperatures (T_d).

exhibits a primary diffraction peak at $2\theta = 5.44°$, with the second-, third-, and fourth-order diffraction peaks when deposited at T_d fixed between 25 and 75 °C, indicating that 3TOIND easily forms well-ordered, layered molecular structures in thin films (Figure 11). On the other hand, only one small diffraction peak was observed at $2\theta = 5.44°$ in the XRD spectrum of the 2TOIND thin film deposited at $T_d = 25$ °C. This oligomer exhibits well-resolved diffraction peaks up to the third-order ($2\theta = 6.58°$, 13.16°, and 19.7°) when deposited at $T_d = 75$ °C meaning that ordered structures in thin films could be obtained by moderate heating of the substrate (Figure 11). It is interesting to note that the *d*-spacings of 3TOIND (16.2 Å) and 2TOIND (13.4 Å) are close to those obtained with 3POIND and 2POIND, respectively. Because the structures of 3TOIND and 2TOIND (aromatic backbone and lateral alkyl side chains) are very similar to those of 3POIND and 2POIND, we suggest from the XRD data that their corresponding thin films have similar packing structures. Consequently, all the 2,8- and 3,9-substituted indolocarbazole derivatives have a favorable molecular orientation for efficient charge transport parallel to the SiO_2 semiconductor interface. It should be noted that the SiO_2 surface pretreatment with hexamethyldisilazane (HMDS) or octyltrichlorosilane (OTS) molecules does not have a significant effect on the XRD patterns of these oligomers.

The use of OIND and OPIND as semiconductor materials in OFETs has been already published in the literature.[13] However, we have shown above that their different single-crystal structures could explain their different charge carrier mobilities. Thus, it will be interesting to verify if the single-crystal structures are preserved in the thin films (in order to confirm this molecular packing effect). The *d*-spacing calculated from the primary diffraction peak of the OIND thin film (16.85 Å) is a little longer than the *a*-axis length (15.26 Å) observed in the single-crystal structure (Figure 4). However, the thin film structure could be similar to one observed in the single crystal if the alkyl side chains are slightly less interdigitated. In the case of OPIND, the vacuum-deposited thin film XRD spectrum reveals the signature of two different structures: a major one at $2\theta = 3.26°$ (*d*-spacing 24.38 Å) and a minor one at $2\theta = 5.48°$ (*d*-spacing 16.05 Å).[13] On the basis of our single-crystal data, only the minor peak at $2\theta = 5.48°$ could be detected; it is assigned as (0 1 0) meaning that the *ac* planes are parallel to the substrate surface (Figure 5). On the other hand, the HPIND thin film XRD spectrum shows only one set of diffraction peaks up to the fourth-order ($2\theta = 4.22°$, 8.38°, 12.62°, and 18.26°) when deposited at $T_d = 25$ °C (Figure 11). The XRD spectra are similar when HPIND was deposited at higher T_d (50 or 75 °C) or on different substrates (HMDS- or OTS-treated substrate) indicating that only one thin film structure is favorable under these conditions. However, the calculated *d*-spacing (21.0 Å) cannot be attributed to the single-crystal structure, and consequently, the thin film structure is different from the single-crystal one mentioned in Figure 6. Despite that HPIND and OPIND show completely different single-crystal structures, their *d*-

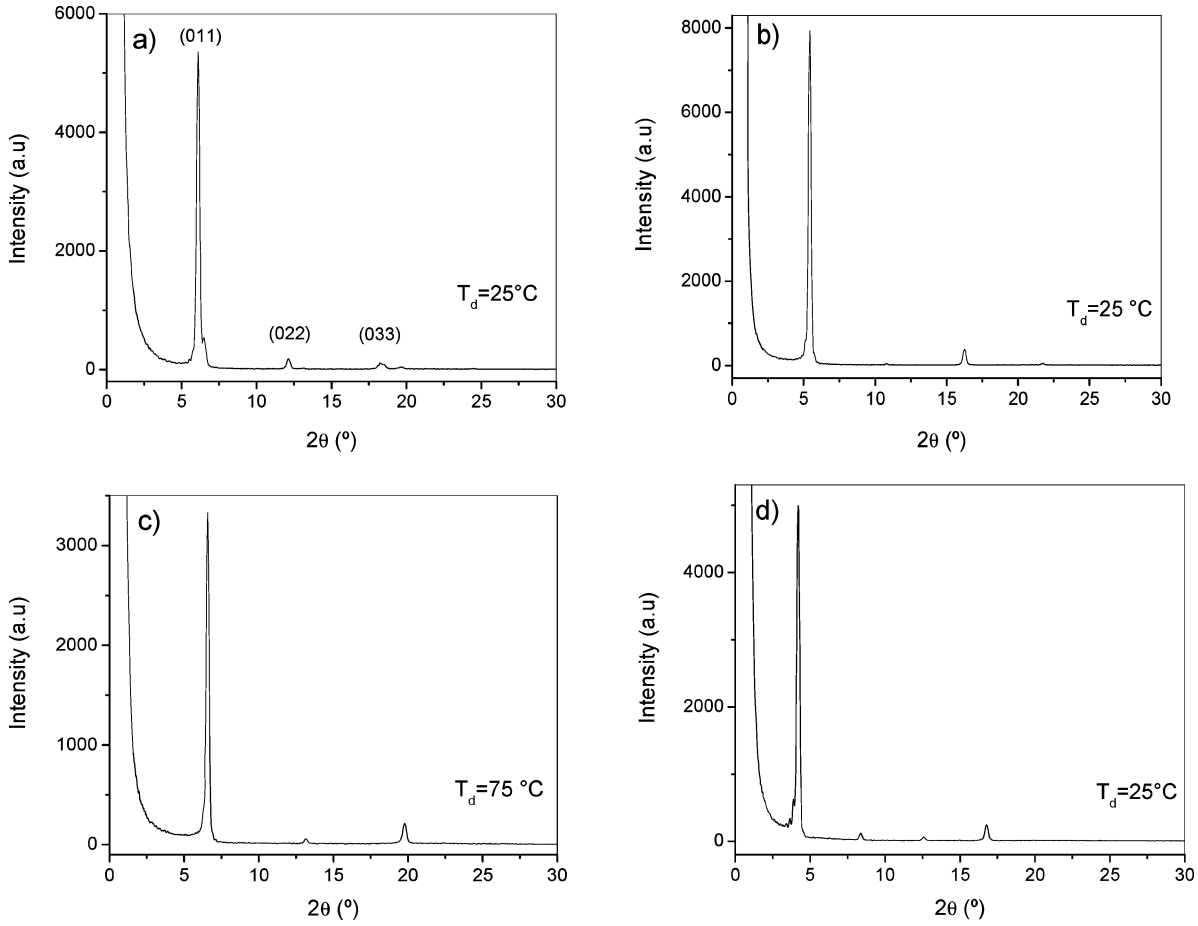

Figure 11. XRD patterns of (a) 2POIND, (b) 3TOIND, (c) 2TOIND, (d) HPIND thin films vacuum-deposited at low substrate temperatures (T_d). OTS-treated SiO_2/Si were used for (a) and (d), HMDS-treated SiO_2/Si for (b) and (c).

spacings in thin films are relatively close (the difference of 3−4 Å is probably due to their different alkyl side chains). We suppose that their thin film structures are quite similar which could be in good agreement with the OFETs results (see below). Finally, we note that the HTIND forms low quality thin films due to its poor crystallization, and therefore it cannot be used in OFETs.

The morphology of vacuum-deposited thin films was also studied by scanning electron microscopy (SEM) in order to obtain more information about the thin-film forming properties of these indolocarbazole derivatives. The films display different crystal morphologies and grain boundaries depending on the oligomer and substrate deposition temperatures. The SiO_2 surface pretreatment with HMDS or OTS molecules has negligible effect on the film morphology. The 3POIND thin film deposited at T_d = 25 °C is made of small interconnected crystal grains with an average length of about 0.5 μm (Figure 12). The grain size increases with increasing T_d; large and long interconnected needle-shaped grains appear at T_d = 75 °C, with an average size of about 0.4 μm × 2 μm. In spite of the fact that the grain size increases, which should usually reduce the grain boundary density, the mobility remains stable. When 3POIND was deposited at T_d = 100 °C a lamellar morphology appeared; the lamellae became smoother and larger at higher T_d but became disconnected (voids and cracks) from each other. The origin of the cracks is probably due to the mismatch in the thermal expansion coefficients of the substrate and the organic semiconductor film.[29] The lamellar morphology observed here is probably related to the appearance of the second set of diffraction peaks in XRD thin film spectra (Figure 10). As a lower mobility was measured with the lamellar morphology, it could be related to a modification in the thin film structure or to the surface coverage of the material.

In the case of 2POIND, the grains obtained at T_d = 25 °C are smaller and less defined than those obtained with 3POIND. When deposited at T_d = 50 °C, the 2POIND film starts to form small interconnected lamellae that shows a positive effect on the electrical property. At higher T_d, the lamellae continue to increase in size and to lose in connectivity without any significant effect on the mobility values until a T_d = 125 °C where the films become completely inactive. The SEM images of 3TOIND resemble those of 3POIND with small interconnected crystal grains at T_d = 25 °C and large smooth lamellae with good continuity at higher T_d. These two different morphologies which have the same XRD spectrum show relatively similar mobilities in this case. The 2TOIND thin films exhibit an irregular granular morphology when deposited at T_d = 25 °C corresponding well to the poorly ordered structure observed in the XRD spectrum. However, a more crystalline lamellar morphology appears at higher T_d, which is in agreement with the XRD and OFETs results. SEM images recorded on HPIND films deposited at T_d = 25 °C display interconnected

(29) Locklin, J.; Ling, M. M.; Sung, A.; Roberts, M. E.; Bao, Z. *Adv. Mater.* **2006**, *18*, 2989−2992.

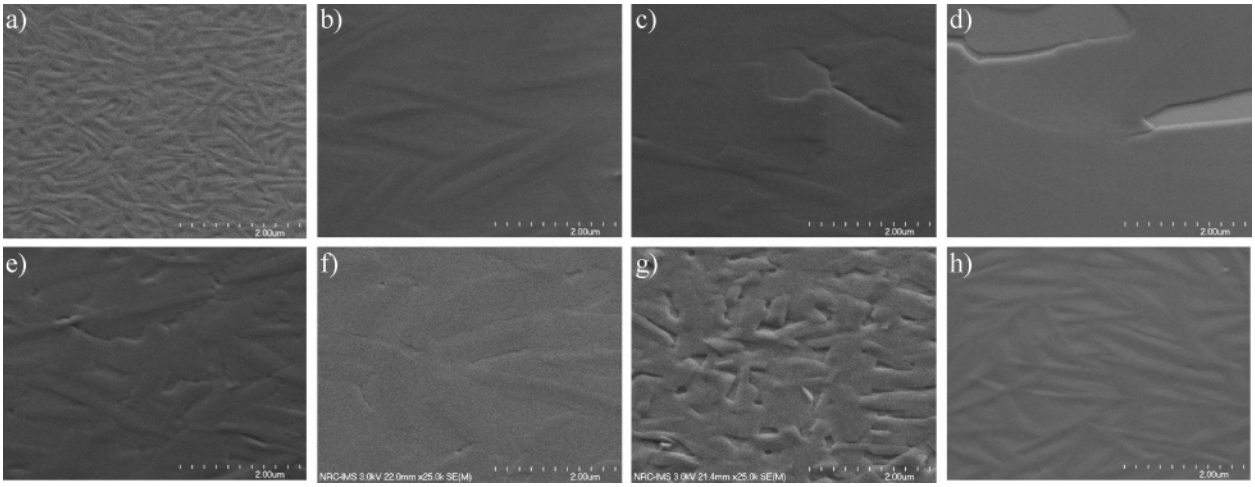

Figure 12. SEM images of 30 nm thin films vacuum-deposited at different substrate temperatures (T_d) on pretreated SiO_2/Si of 3POIND (a) $T_d = 25$ °C (OTS), (b) $T_d = 75$ °C (OTS), (c) $T_d = 100$ °C (OTS), (d) $T_d = 150$ °C (OTS); 2POIND (e) $T_d = 75$ °C (OTS); 3TOIND (f) $T_d = 75$ °C (HMDS); 2TOIND (g) $T_d = 75$ °C (HMDS); and HPIND (h) $T_d = 75$ °C (OTS).

needle-shaped grains with an average length of about 0.8 μm. The grains become longer and larger at $T_d = 50$ °C with an average size of about 0.2 μm × 2 μm.

Field-Effect Transistor Performances. OFETs of these indolo[3,2-*b*]carbazole derivatives were fabricated on SiO_2/Si substrates by high-vacuum evaporation at different substrate temperatures using a top-contact device configuration. Different pretreated SiO_2/Si substrates that were subject to various surface treatments [bare, hexamethyldisilazane (HMDS), and octyltrichlorosilane (OTS)] were investigated to evaluate the effect of gate dielectric surface pretreatment on the performances of the OFET devices. The electrical measurements were performed inside a dark box at room temperature and under ambient atmosphere. All indolo[3,2-*b*]carbazole derivatives behave as p-type organic semiconductors with well-defined linear and saturation regimes. For example, Figure 13 represents the source-drain current (I_{DS}) versus source-drain voltage (V_{DS}) characteristics for an OFET made with 3POIND at various gate voltages (V_G). The hole mobilities calculated in the saturation regime, the on/off current ratios, and the threshold voltages obtained at different T_d values are summarized in Table 3. As expected, the surface modification to the SiO_2 prior to the deposition is very important. For all these oligomers, the HMDS- and OTS-treated substrates exhibit better mobilities and on/off current ratios than the bare SiO_2 no matter what substrate temperature was used during the deposition. As the XRD analysis and SEM have revealed a limited effect of the substrate pretreatment on the thin-film structures and morphologies, this difference in performances is probably related to the chemical and electrical properties of the gate dielectric surface. In fact, it was demonstrated that the accumulation layer in OFETs resides in the first few deposited monolayers,[30] and consequently the roughness and the chemical modification of the gate dielectric surface before semiconductor deposition have a great impact on the performances of the devices.[31] For example, the utilization of silane agents, like HMDS and OTS, can lower

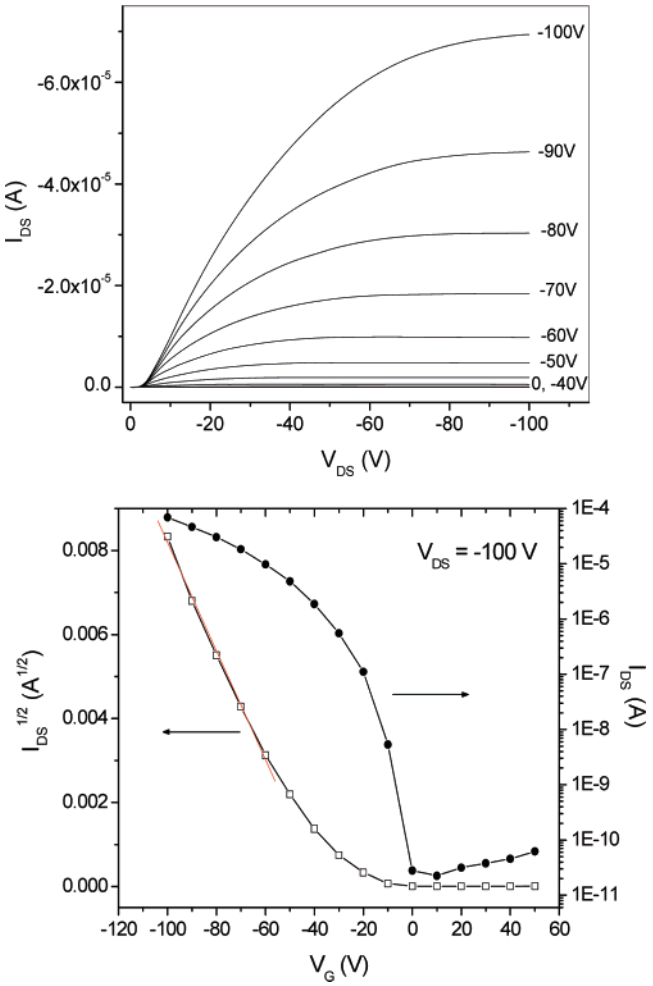

Figure 13. Source-drain current (I_{DS}) versus source-drain voltage (V_{DS}) at various gate voltages (V_G) for top-contact field effect transistors using 3POIND deposited at $T_d = 75$ °C on OTS-treated SiO_2. The transfer characteristics in the saturation regime at a constant source-drain voltage ($V_{DS} = -100$ V) are also included.

the surface conductivity of the dielectric[32] which would minimize the off current and therefore increase the on/off current

(30) (a) Dinelli, F.; Murgia, M.; Levy, P.; Cavallini, M.; Biscarini, F.; Leeuw, D. M. d. *Phys. Rev. Lett.* **2004**, *92*, 116802-4. (b) Ruiz, R.; Papadimitratos, A.; Mayer, A. C.; Malliaras, G. G. *Adv. Mater.* **2005**, *17*, 1795−1798.

(31) (a) Salleo, A.; Chabinyc, M. L.; Yang, M. S.; Street, R. A. *Appl. Phys. Lett.* **2002**, *81*, 4383−4385. (b) Shtein, M.; Mapel, J.; Benziger, J. B.; Forrest, S. R. *Appl. Phys. Lett.* **2002**, *81*, 268−270.

(32) Voorthuyzen, J. A.; Keskin, K.; Bergveld, P. *Surf. Sci.* **1987**, *187*, 201−211.

Table 3. Field-Effect Mobility (μ), On/Off Current Ratios (I_{on}/I_{off}), and Threshold Voltage (V_T) of Indolocarbazole Derivatives Vacuum-Deposited on Differently Treated SiO_2 Surfaces and at Different Substrate Temperatures (T_d).

oligomer	SiO_2	μ ($cm^2\ V^{-1}\ s^{-1}$)	I_{on}/I_{off}	V_T (V)	μ ($cm^2\ V^{-1}\ s^{-1}$)	I_{on}/I_{off}	V_T (V)	μ ($cm^2\ V^{-1}\ s^{-1}$)	I_{on}/I_{off}	V_T (V)
		$T_d = 25$ °C			$T_d = 75$ °C			$T_d = 100$ °C		
3POIND	OTS	0.20	1×10^6	−59	0.20	5×10^6	−55	0.09	5×10^6	−36
2POIND	OTS	0.01	5×10^5	−54	0.04	1×10^6	−54	0.06	2×10^6	−49
3TOIND	HMDS	0.02	1×10^6	−62	0.03	1×10^6	−56	0.02	1×10^6	−51
2TOIND	HMDS	0.001	1×10^5	−26	0.015	1×10^6	−34		no field effect	
		$T_d = 25$ °C			$T_d = 50$ °C			$T_d = 75$°C		
HPIND	OTS	0.04	1×10^5	−57	0.11	5×10^4	24	0.04	5×10^4	−46
OPIND[a]	OTS	0.02	1×10^6	−	0.12	1×10^7	−7	−	−	−

[a] Best performances of OPIND reported in ref 13.

ratio.[26] On the other hand, as detailed in the Supporting Information, the procedures used for the preparation of bare as well as HMDS- and OTS-pretreated SiO_2 allowed us to obtain a smooth surface.

The 3POIND shows a hole mobility as high as 0.2 $cm^2\ V^{-1}\ s^{-1}$ and an on/off current ratio of 10^6 when deposited at T_d = 25 °C on OTS-treated substrate. These performances are among the best results reported in the literature for OFETs prepared without heating of the substrate during the evaporation. As shown in Table 3, the hole mobility of 3POIND remains stable at T_d = 75 °C and then begins to decrease at higher T_d. These results are not surprising; as demonstrated by the X-ray analysis, 3POIND thin films show a highly ordered structure at low T_d, similar to the single-crystal one, with an appropriate orientation of the molecules on the substrate. Also, the lower mobility observed starting from T_d = 100 °C could be related, as shown by thin film XRD analysis and SEM images, to the formation of new thin-film structures, where the 3POIND molecules are more tilted relative to the substrate surface or/and to the appearance of voids and cracks under elevated T_d. Interestingly, when deposited at T_d between 25 and 75 °C on an HMDS-treated substrate, the 3POIND exhibited a constant mobility and an on/off current ratio of 0.12 $cm^2\ V^{-1}\ s^{-1}$ and 10^6, respectively. Further increase of the substrate temperature resulted in lower mobilities, as observed with OTS-treated substrates.

The 2POIND deposited at T_d = 25 °C on OTS-treated substrates shows a mobility of 0.01 $cm^2\ V^{-1}\ s^{-1}$ which is about 1 order of magnitude lower than the one obtained with 3POIND. When the substrate temperature was increased for the thin film deposition of 2POIND, the hole mobility improved and reached a maximum of 0.06 $cm^2\ V^{-1}\ s^{-1}$ at T_d = 100 °C. On the basis of the XRD analysis and the SEM images of thin films, this mobility increase can be attributed to the formation of interconnected lamellae rather than to a modification of the thin film structure. Table 3 also shows that the 3POIND performances are always better than those obtained with 2POIND. This difference cannot be explained only by their morphology difference; the packing mode of 2POIND, which is less efficient, plays an important part here, as we have proposed by the single-crystals XRD analysis. Also, we note that the 2POIND performances obtained with HMDS-treated substrates were about 2 times lower than those obtained with OTS-treated ones.

The 3TOIND has a relatively stable mobility, about 0.02 $cm^2\ V^{-1}\ s^{-1}$, when the substrate temperature is fixed between 25 and 125 °C. On the other hand, the 2TOIND mobility shows a strong dependence on the substrate temperature used during the evaporation. At T_d = 25 °C, the mobility was about 0.001 $cm^2\ V^{-1}\ s^{-1}$, and it reached 0.015 $cm^2\ V^{-1}\ s^{-1}$ at T_d = 75 °C. Interestingly, the OFET performances obtained with 3TOIND and 2TOIND are in good agreement with the XRD analysis and SEM results detailed previously. In the case of 3TOIND and 2TOIND, the HMDS-treated substrates showed hole mobilities about 1 order of magnitude higher than those obtained with the OTS-treated ones. This study shows that the performances of the phenyl-substituted indolo[3,2-*b*]carbazole derivatives are clearly better than those obtained with their corresponding thiophene indolocarbazole derivatives. This difference is probably due to the increased crystallinity of the phenyl-substituted indolo[3,2-*b*]carbazole derivatives; unfortunately without the single-crystals analysis of 3TOIND and 2TOIND, it is difficult to confirm the exact role of the molecular packing and intermolecular interactions here. In the case of HPIND, the grain size (see SEM images) seems to have an important impact on the mobility; the film deposited at T_d = 25 °C shows a mobility of 0.04 $cm^2\ V^{-1}\ s^{-1}$, while the mobility obtained at T_d = 50 °C was 0.11 $cm^2\ V^{-1}\ s^{-1}$. Both HPIND and OPIND exhibit a similar optimal mobility at T_d = 50 °C, which confirms our suggestion concerning the similarity of their thin film structures, even with their completely different single-crystal structures. Finally, this study clearly shows that the substitution of the indolo[3,2-*b*]carbazole core with a phenyl unit such as 3POIND is an effective strategy to improve the performances of this class of materials, and according to the single-crystals analysis, the molecular packing and the intermolecular interactions play a major role in this improvement.

In order to test the stability of the organic transistors, we have measured the hole mobilities and on/off ratio periodically for 5 months. The devices were characterized under the same conditions described above and stored under a nitrogen atmosphere and light (wavelengths <500 nm removed by filtration) between two measurements. As shown in Figure 14, after 5 months, the mobility of 3POIND, deposited on OTS-treated substrate at T_d = 75 °C, remains higher than 0.1 $cm^2\ V^{-1}\ s^{-1}$ and the on/off current ratio is still around 10^7. All the devices prepared with 3POIND show excellent stability, no matter what kind of substrate was used (bare, HMDS-, or OTS-treated) or what substrate temperature was applied during the deposition.

In the case of 2POIND, the performances of the devices prepared with OTS-treated substrates are very stable. For example, the mobility and the on/off current ratio of 2POIND deposited on OTS-treated substrate at T_d = 100 °C were maintained, after 3 months, at about 0.05 $cm^2\ V^{-1}\ s^{-1}$ and 4×10^6, respectively (see Table 3 for comparison). On the other hand, when the 2POIND was deposited on bare Si/SiO_2, an important decrease of the mobility (2 to 4 times) and the on/off current ratio (about 2 orders) has been observed which could

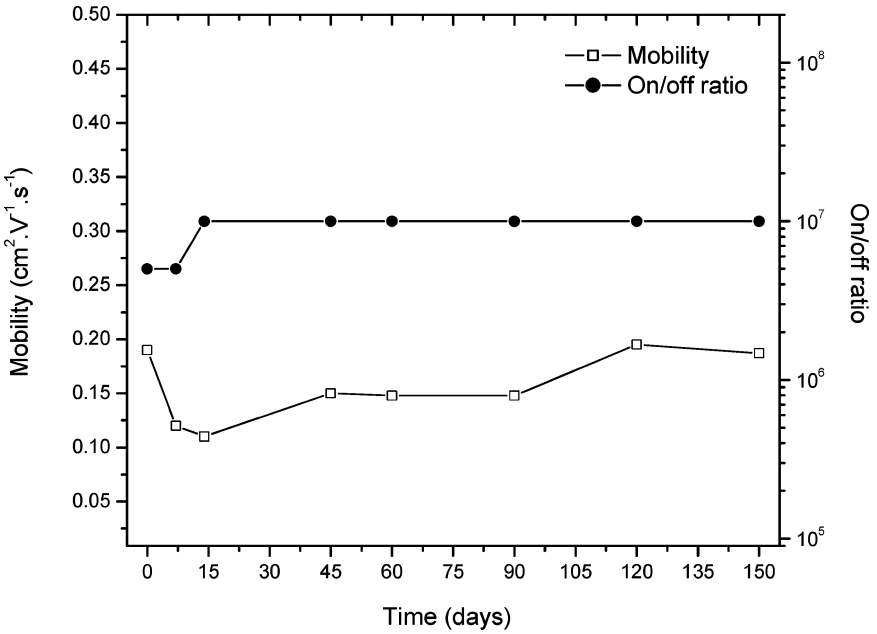

Figure 14. Field-effect mobility and on/off current ratio of devices based on 3POIND tested over a period of 5 months.

be attributed to chemical modification at the interface between the semiconductor and the gate dielectric. The variations of the mobility and of the on/off current ratio are less important with HMDS-treated substrates. The thiophene-substituted indolocarbazoles also show good environmental stability. For example, in the case of 3TOIND deposited on HMDS-treated substrates at $T_d = 75$ °C, the hole mobility and the on/off current ratio remain stable at about 0.03 $cm^2\ V^{-1}\ s^{-1}$ and 10^6, respectively, even after 15 months of storage. Finally, we note that all the devices prepared with HPIND do not show any important change in the mobility or the on/off current ratio after 3 months of storage. The results obtained here indicate that OFETs based on these indolo[3,2-*b*]carbazole derivatives have excellent environmental stability which could be related to the large band gap and low HOMO energy level of these oligomers.

Conclusion

In this report, new phenyl- or thienyl-substituted indolo[3,2-*b*]carbazoles have been synthesized and their thermal, electrochemical, structural, and hole-transport properties were investigated. Careful and complete X-ray analyses have revealed the importance of the length of the alkyl chain linked on the nitrogen atoms to obtain an efficient molecular packing. Moreover, the addition of aromatic substituents, as either lateral chains or end groups, creates shorter contacts between adjacent molecules which enable two- or three-dimensional networks with better hole mobility. For instance, a hole mobility as high as 0.2 $cm^2 \cdot V^{-1} \cdot s^{-1}$ and an on/off ratio of 10^6 were obtained when 3,9-diphenyl-5,11-dioctylindolo[3,2-*b*]carbazole was used as an active layer in an OFET. It has also been observed that the molecules in the active layer deposited by high-vacuum evaporation are generally packed in the same way as those observed in the single-crystal structures, with the long axis of the molecule being parallel to the substrate and their alkyl chain pointing vertically. Finally, the stability of the devices was tested, and no lowering of the field-effect mobility was observed even after 5 months. Future work will focus on the evaluation of the performances of single crystals in OFETs as well as solution-processed thin films since these materials are easily crystallizable and processable and show superior stability in air. These studies should therefore lead to the development of new electroactive and photoactive pentacene-like materials with improved processability and stability.

Acknowledgment. This work was supported by discovery and strategic grants from the Natural Sciences and Engineering Research Council (NSERC) of Canada. The authors acknowledge Prof. F.-G. Fontaine for useful discussions.

Supporting Information Available: Details of syntheses, characterization, device fabrication and testing (pdf), and X-ray crystallographic information files of 2POIND, 3POIND, HPIND, HTIND, OPIND, and OIND (CIF). This material is available free of charge via the Internet at http://pubs.acs.org.

JA071923Y